

## Article

# Novel DQ-Based Multicarrier PWM Strategy for a Single-Phase F-Type Inverter

Raad Abdullah <sup>1,\*</sup>, Mouna Ben Smida <sup>1</sup>, Ali Thamallah <sup>1</sup>, Aouse Khalaf <sup>2</sup> and Anis Sakly <sup>1</sup>

<sup>1</sup> National Engineering School of Monastir (ENIM), University of Monastir, Ibn El Jazzar, Skaness, Monastir 5019, Tunisia; mouna\_bensmida@yahoo.fr (M.B.S.); ali.thamallah@isetkr.run.tn (A.T.); sakly\_anis@yahoo.fr (A.S.)

<sup>2</sup> Engineering Faculty, Sakarya University, Sakarya 54050, Turkey; aouse.khalaf@ogr.sakarya.edu.tr

\* Correspondence: eng.raaddhahi79@gmail.com

**Abstract:** This paper presents a novel DQ-based multicarrier pulse width modulation PWM for a single-phase, three-level PV-powered grid-connected F-type inverter. The main control objective in the proposed inverter is to regulate the grid current with low total harmonic distortion and load power components compensation. Despite the F-type inverter's advanced advantages, there are only a few works addressing the control issue in the literature yet. The proposed control and switching methods aim to achieve both DC-side voltage balance and the lowest switching losses. The proposed scheme has been designed based on a modified multicarrier PWM switching algorithm. Consequently, the proposed control method is able to satisfy the requirements of DC-side voltage balance and achieve lower switching losses. A further advantage of the proposed control and switching methods is that they retain the main advantage of the F-Type inverter, which is that only 25% of the power switches are exposed to full DC voltage. This is an important advantage since it reduces the overall cost of the inverter and improves its reliability. Overall, the proposed modified multicarrier PWM switching algorithm appears to be a promising approach for controlling the F-Type inverter, offering improved performance and efficiency compared to other control methods. The theoretical model was verified through simulation using MATLAB/Simulink. According to the simulation results, the grid current and dc capacitor voltages are successfully managed in all operational situations.

**Keywords:** DQ-based control; F-type inverter; PV-powered inverter



**Citation:** Abdullah, R.; Smida, M.B.; Thamallah, A.; Khalaf, A.; Sakly, A. Novel DQ-Based Multicarrier PWM Strategy for a Single-Phase F-Type Inverter. *Electronics* **2023**, *12*, 2972. <https://doi.org/10.3390/electronics12132972>

Academic Editor: Cheng Siong Chin

Received: 30 May 2023

Revised: 25 June 2023

Accepted: 30 June 2023

Published: 6 July 2023



**Copyright:** © 2023 by the authors. Licensee MDPI, Basel, Switzerland. This article is an open access article distributed under the terms and conditions of the Creative Commons Attribution (CC BY) license (<https://creativecommons.org/licenses/by/4.0/>).

## 1. Introduction

The proliferation of electric vehicle charging stations and the increase in non-linear loads can have negative impacts on the power system in cases where there is no efficient power management. Non-linear loads can introduce harmonic distortions, which can affect the voltage and frequency of the power system [1]. Power quality is a critical aspect of power systems, and improving it is essential, particularly in grids that contain nonlinear loads [2]. Nonlinear loads, such as electronic equipment, cause harmonic distortion in the power system, which can lead to problems such as reduced efficiency, increased losses, and even equipment failure [3]. Photovoltaic (PV) array systems can help improve power quality thanks to the voltage source converter (VSC) that is at the heart of the PV system [4]. The VSC is a power electronics device that can control the voltage and the frequency of the PV system [5], allowing it to respond to changes in load demand. By adjusting the real power output of the PV system, the VSC can compensate for the distortion caused by nonlinear loads, helping to maintain a stable voltage and high-quality power systems.

While using PV inverters to compensate for the power components in the electrical grid, it is very important to the system efficiency as high as possible. The literature reports that the proliferation of multilevel inverters and their associated controls have led to significant improvements in several industrial applications [6]. For example, in motor

drives, multilevel inverters have been shown there is a significant reduction in torque ripple and improvement in motor efficiency, which can lead to significant energy savings. In renewable energy systems, multilevel inverters can improve the quality of the output voltage, which can enhance the performance of photovoltaic systems and wind turbines [7]. In power grid applications, multilevel inverters can improve the power quality and stability of the grid, which can reduce power outages and improve overall reliability [8]. Among the wide range of inverters, there is the F-type inverter which was introduced for the first time by Charles I. Odeh et al. [9]. It is the best due to its low cost and low switching losses. The three-phase F-type inverter's switching method and operating concept have been detailed in [9]. This inverter incurs additional costs and losses due to the lower voltage stress placed on each leg's three power switches.

Low total harmonic distortion (THD) in the grid current, quick dynamic response, and resilience to perturbations in input and output variables are typical control goals for a grid-connected inverter [10]. Many control techniques were used by the researchers to control the grid-connected inverters, like fuzzy logic control [11], synthetic inertia control [12], predictive control [13], etc. The main drawback of those control systems is the absence of dealing with nonlinear loads as well as PV power inversion at the same time as done in the current paper.

To handle the AC systems commonly employed in the market, the utilization of DC-AC converters or a combination of AC-DC converters and DC-AC converters is necessary to convert renewable energy into AC power. Consequently, DC-AC converters play a crucial role in today's industry. Multilevel DC-AC converters utilize switching paths to generate an output voltage that exhibits a hierarchical pattern. By incorporating additional levels or filters, the output voltage can resemble a sine wave. The output voltage produced by the multi-stage DC-AC converter is stratified, ensuring that the voltage stress on the switch is controlled. As a result, it becomes possible to achieve high-voltage AC output using a switch with low-voltage stress [14].

Multilevel inverters (MLI) have gained significant attention from academia and the research community in recent times, primarily due to their suitability for high- and medium-power applications. Multilevel inverters offer several advantages over traditional two-level inverters, such as improved voltage waveform quality, reduced harmonic distortion, lower electromagnetic interference (EMI), and increased power capability [15].

One of the key advantages of multilevel inverters is their ability to operate at higher voltage levels while using lower voltage-rated components. This reduces the stress on the power switches and capacitors, improving the overall system reliability and efficiency.

MLI systems are designed to improve efficiency and reduce the harmonic distortion of power conversion, compared to traditional two-level inverters [16,17]. Cascaded H-Bridge (CHB) MLI structures are commonly used in interfacing with photovoltaic (PV) systems due to their ability to provide higher reliability and easy modularity. The CHB MLI requires multiple isolated DC sources in each H-bridge. This makes it highly suitable for PV (photovoltaic) applications, as individual PV panels can be used in each H-bridge along with distributed maximum power point tracking (DMPPT) control [18–20].

Switching losses in inverters reduces the system efficiency and increases the switches' cost due to the high rating. Many researchers proposed soft switching techniques to reduce the losses and succeeded in loss reduction, but the overall system cost increased, and the control complex [21]. In this work, soft switching is included in the main control algorithm without any additive components or control complexity.

DC capacitors' voltage balancing is essential in controlling the modern multilevel inverters NPC, T-type, and F-type inverters [22]. When compared to other multilevel topologies, the NPC (Neutral-Point-Clamped) family stands out due to its requirement of only one shared DC voltage source for all converter legs. This design offers the advantage of employing a complete semiconductor layout, with the capacitors needed to be placed outside the converter legs. Unlike passive components, which are typically larger in size compared to semiconductors, this configuration avoids the inclusion of bulky elements

within the converter legs. As a result, it becomes feasible to create a more compact converter implementation, reducing its volume and increasing the power density [23]. The balance of capacitor voltages in the NPC converter relies on various factors, including the amplitude modulation index, frequency modulation index, and the power factor of the load [24].

In this work, as explained in Section 2, the capacitors' voltage level balancing is included with the main control algorithm.

The increasing penetration of nonlinear loads in power systems has led to various issues, such as (i) harmonic distortion: nonlinear loads introduce harmonic currents into the grid, which can lead to voltage distortion and interfere with the operation of other connected devices. Harmonic distortion can cause overheating in transformers, capacitors, and other equipment, leading to premature failure and increased energy losses [25]. (ii) Reactive power demand: nonlinear loads often exhibit reactive power consumption, which can result in an increased demand for reactive power from the grid. This can lead to voltage drops, reduced system efficiency, and additional stress on power generation and transmission equipment [26]. (iii) Poor power factor: nonlinear loads tend to have a lagging power factor, which means that they consume more reactive power compared to their real power consumption. This can result in a decreased overall power factor for the grid, leading to increased losses, reduced system capacity, and additional costs for utilities [27]. (iv) Voltage Fluctuations: nonlinear loads, especially those with high switching frequencies, can cause rapid voltage fluctuations and transient disturbances in the grid. These fluctuations can affect the operation of sensitive equipment and lead to performance issues or even equipment damage [28]. Additionally, (v) electromagnetic interference (EMI): nonlinear loads can generate high-frequency noise and electromagnetic interference, which can interfere with the proper functioning of nearby electronic devices and communication systems [29]. These problems can adversely affect the quality and efficiency of electrical power distribution. To address these challenges, this research proposes a novel approach that focuses on utilizing grid-connected PV array for compensating the power components associated with nonlinear loads.

This paper is organized as follows: F-type inverter modeling is performed in Section 2. The proposed control method is presented in Section 3. The simulation results discussion is given in Section 4. Finally, the conclusions are set out in Section 5.

## 2. F-Type Inverter Modeling

An F-type inverter was proposed first in [9] as a three-level inverter with minimum switching states (9 states only). Figure 1 shows the single-phase F-type inverter model.

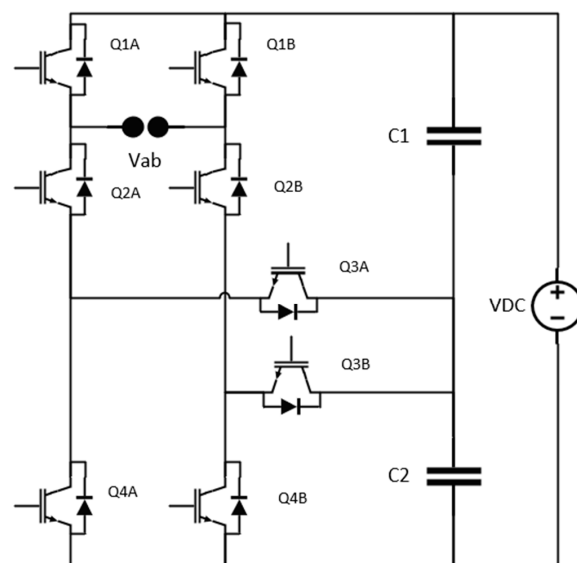


Figure 1. F-type single-phase inverter model.

F-type inverter output voltage expression is given in Equation (1):

$$V_{ab} = (Q_{1A} - Q_{1B})V_{C1} + (Q_{3A} - Q_{3B})V_{C2} \tag{1}$$

where:

$V_{ab}$ : inverter output voltage.

$Q_{mn}$ :  $mn$  IGBT gate state (0 or 1),  $m$ : IGBT number,  $n$ : Leg (A or B)

The switching cases and related output voltages are listed in Table 1, while the inverter active path for each switching case are shown in Figure 2.

**Table 1.** The switching cases and related output voltages. (\*: letters represent switching cases in Figure 2).

Switching State *	S <sub>1a</sub>	S <sub>2a</sub>	S <sub>3a</sub>	S <sub>4a</sub>	S <sub>1b</sub>	S <sub>2b</sub>	S <sub>3b</sub>	S <sub>4b</sub>	V <sub>ab</sub>
1 (g)	ON	OFF	ON	OFF	ON	OFF	ON	OFF	0
2 (a)	ON	OFF	ON	OFF	OFF	ON	ON	OFF	$V_{C1} = (\frac{V_{dc}}{2})$
3 (b)	OFF	ON	ON	OFF	OFF	ON	OFF	ON	$V_{C2} = (\frac{V_{dc}}{2})$
4 (c)	ON	OFF	ON	OFF	OFF	ON	OFF	ON	$V_{dc}$
5 (i)	OFF	ON	ON	OFF	OFF	ON	ON	OFF	0
6 (d)	OFF	ON	ON	OFF	ON	OFF	ON	OFF	$-V_{C2} = (\frac{-V_{dc}}{2})$
7 (e)	OFF	ON	OFF	ON	OFF	ON	ON	OFF	$-V_{C2} = (\frac{-V_{dc}}{2})$
8 (f)	OFF	ON	OFF	ON	ON	OFF	ON	OFF	$-V_{dc}$
9 (h)	OFF	ON	OFF	ON	OFF	ON	OFF	ON	0

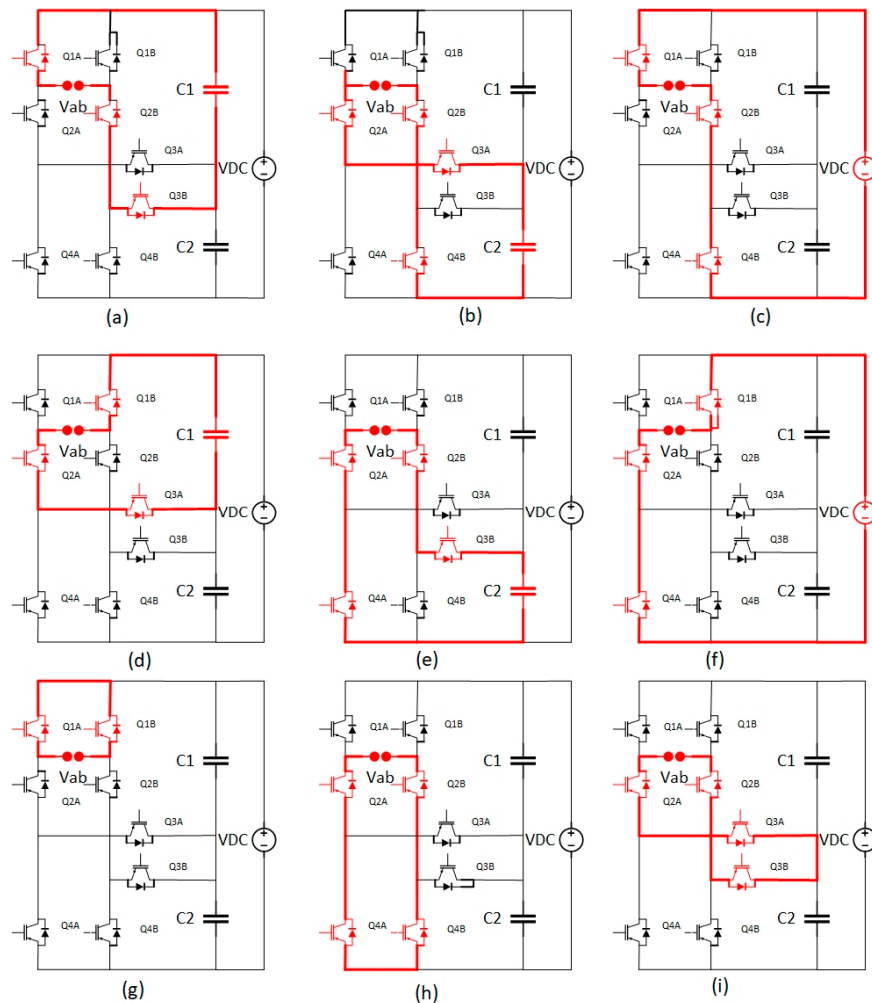


**Figure 2.** F-type inverter switching cases (a–i) show the active elements in F-type inverter.

### 3. Proposed Method

DQ control, also known as the Clarke–Park transformation, is a common control strategy used in inverters for driving three-phase alternating current (AC) motors. It is primarily employed in motor drives that utilize field-oriented control (FOC) or vector control techniques [30]. The purpose of DQ control is to decouple the control of the motor's torque and flux components. By transforming the three-phase AC currents or voltages into a two-coordinate reference frame, the studied method allows independent control of the torque-producing (D-axis) and flux-producing (Q-axis) components. In the classical orientation of the reference frame, torque is shaped by q-axis current and flux by d-axis current.

In a single-phase inverter, the DQ control strategy can be used to regulate both the active (real) and reactive (imaginary) currents. By applying DQ analysis, the single-phase quantities can be transformed into a two-coordinate reference frame, where the D-axis represents the active current component and the Q-axis represents the reactive current component [31]. Here's how DQ analysis can be used to control active and reactive currents in a single-phase inverter. Signal Transformation: The single-phase current or voltage signal is transformed from the time domain to the DQ reference frame using the Clarke transformation and the Park transformation [32].

- a- Clarke Transformation: The single-phase current or voltage is converted into two orthogonal components, typically referred to as the alpha and beta components.
- b- Park Transformation: The alpha and beta components obtained from the Clarke transformation are transformed into the DQ reference frame. The Park transformation involves rotating the alpha-beta frame by an angle equal to the desired reference frame angle.

The proposed control method is a combination of DQ control and modified multicarrier PWM techniques to control grid connect F-type inverter and satisfy PV power utilization and grid power component compensation. The load and grid currents were analyzed to obtain the modulated control signal. Grid current alpha-beta conversion expressed in Equation (2):

$$\begin{bmatrix} i_g \alpha \\ i_g \beta \end{bmatrix} = \begin{bmatrix} i_g(\omega t + \varnothing) \\ i_g(\omega t + \varnothing + \frac{\pi}{2}) \end{bmatrix} \quad (2)$$

While the D-Q components for the grid current are expressed in Equation (3):

$$\begin{bmatrix} i_g d \\ i_g q \end{bmatrix} = \begin{bmatrix} \sin(\omega t) & -\cos(\omega t) \\ \cos(\omega t) & \sin(\omega t) \end{bmatrix} \begin{bmatrix} i_g \alpha \\ i_g \beta \end{bmatrix} \quad (3)$$

The load current D-Q components are obtained in the same way; see Equations (4) and (5):

$$\begin{bmatrix} i_L \alpha \\ i_L \beta \end{bmatrix} = \begin{bmatrix} i_L(\omega t + \varnothing) \\ i_L(\omega t + \varnothing + \frac{\pi}{2}) \end{bmatrix} \quad (4)$$

$$\begin{bmatrix} i_L d \\ i_L q \end{bmatrix} = \begin{bmatrix} \sin(\omega t) & -\cos(\omega t) \\ \cos(\omega t) & \sin(\omega t) \end{bmatrix} \begin{bmatrix} i_L \alpha \\ i_L \beta \end{bmatrix} \quad (5)$$

The grid Q-axis (reactive and distorted) current components are forced to be zero by using Equation (6):

$$i_g^* q = 0 \quad (6)$$

While the D-axis current component equals the difference between the load D-axis current component and the PV array current as expressed in Equation (7):

$$i_g^* d = i_L d - I_{PV} \quad (7)$$

In the F-type inverter, both grid current and DC-side capacitors voltage should be controlled in such a way as to minimize grid current distortion and keep DC-side capacitors'

voltages balanced. Therefore, the F-type inverter cannot be driven by the traditional multicarrier PWM technique, which leads to the proposed special driving algorithm. The proposed switching algorithm is described in the flowchart shown in Figure 3.

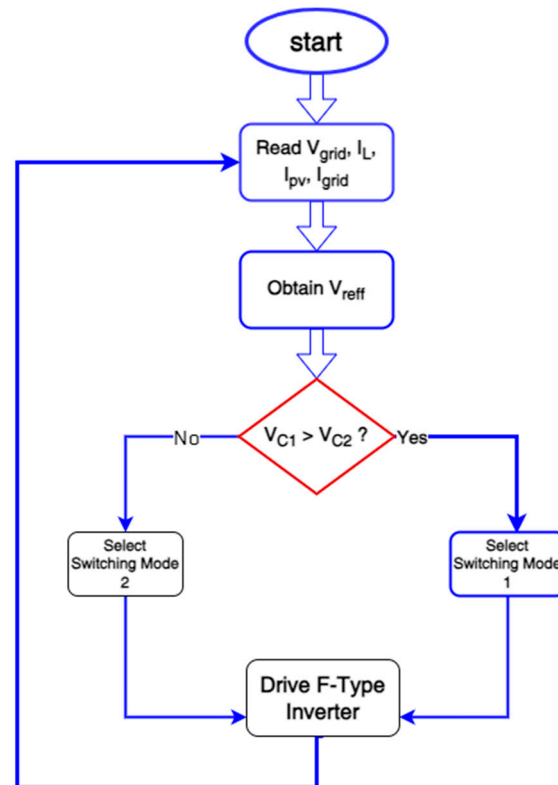


Figure 3. GCFTPV working flowchart.

When the modulated voltage signal is obtained (for minimum grid current distortion), the next step is to check which capacitor voltage is the highest. Depending on the voltage level test, the switching mode is selected. This procedure ensures voltage balance for DC-side capacitors without needing extra components. DC-side capacitors voltage balance keeps output AC voltage symmetry.

#### 4. Simulation Results Discussion

The simulation results of the proposed system are presented in this section. Firstly, the switching signals are examined for three different scenarios of PV behavior. The first scenario, which focuses on the idle PV array, is discussed in Section 4.1. The second scenario ( $P_{pv} < P_{load}$ ) is covered in Section 4.2, while the third scenario addressing  $P_{pv} > P_{load}$  is explained in Section 4.3. Section 4.4 delves into the discussion of the impact of sudden load changes, and Section 4.5 explores the effect of changes in the power output of the PV array. Finally, in Section 4.6, a comparison is made between the performances of F-type and T-type inverters using the proposed control scheme.

The proposed system is simulated for many operating cases depending on the real power produced by the PV array. Figure 4 shows the reference and carrier waveforms. The first carrier amplitude varies between  $-1$  and  $-0.5$ , the second carrier amplitude varies between  $-0.5$  and zero volt, the third carrier amplitude varies between zero and  $0.5$ , and finally, the fourth carrier amplitude varies between  $0.1$  and  $1$ . Thus, the modulated reference signal amplitude can be varied between  $-1$  and  $1$ . PWM signal generates by comparing each carrier signal with the reference signal used for controlling.

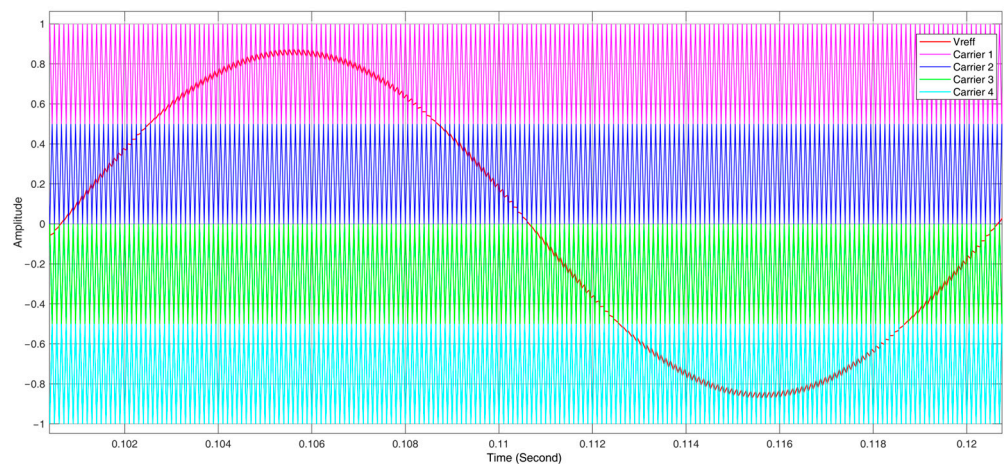


**Figure 4.** Reference and carrier waveforms (each color represents carrier waveform, while the red colored curve represents the reference signal).

Keeping the main capacitors' voltage equilibrium is the key to generating three-level voltage by the F-type inverter. Additionally, the proposed method keeps the other main advantage of the F-type inverter, which is that the voltage stress applied on 25% of the inverter switch only is equal to the main DC supply voltage, while the other 75% work with only 50% of the DC supply voltage as shown in Figure 5. Another advantage of the proposed method is the lowest switching losses despite using the PWM switching technique, as shown in Figure 6.

As shown in Figures 5 and 6, it is clear that three of the switches are working in zero current switchings and two switches are working with low switching losses while the other three switches are working in normal operating, and also the switching losses are low compared with traditional PWM based inverters losses.

The generated voltage by the F-type inverter, depending on the proposed switching method, is three shown in Figure 7. In the same figure, the main capacitors' voltages curves are shown.

For all simulated cases, the grid current still has a unity power factor with minimum total harmonic distortion (THD).

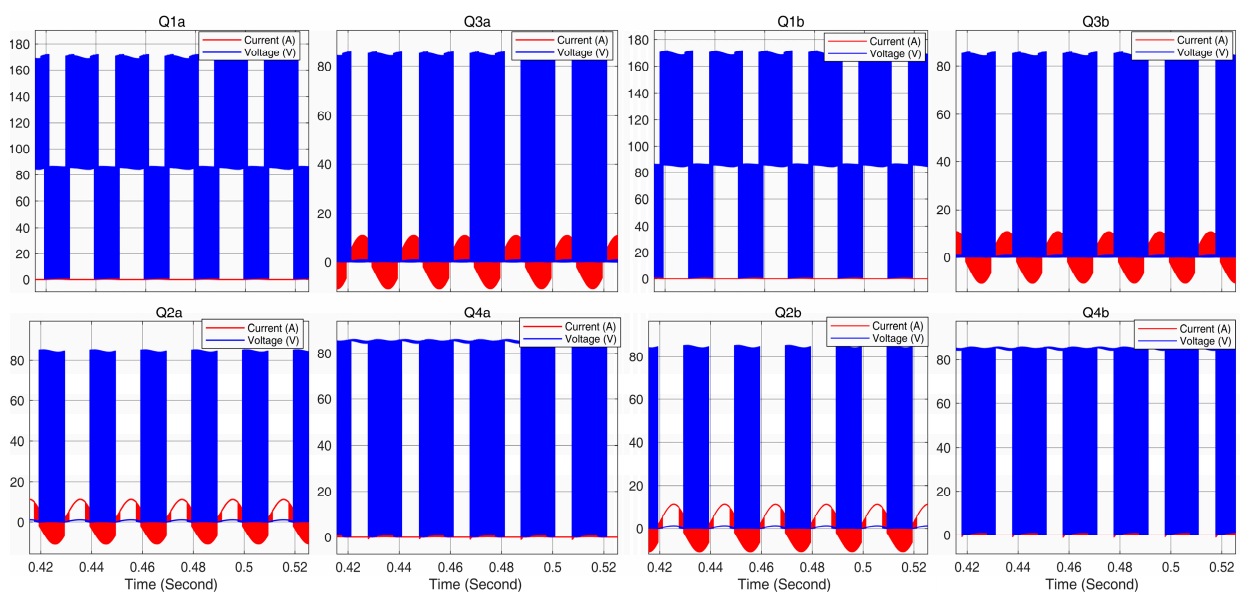


**Figure 5.** Voltage stress on each switch in the proposed system.

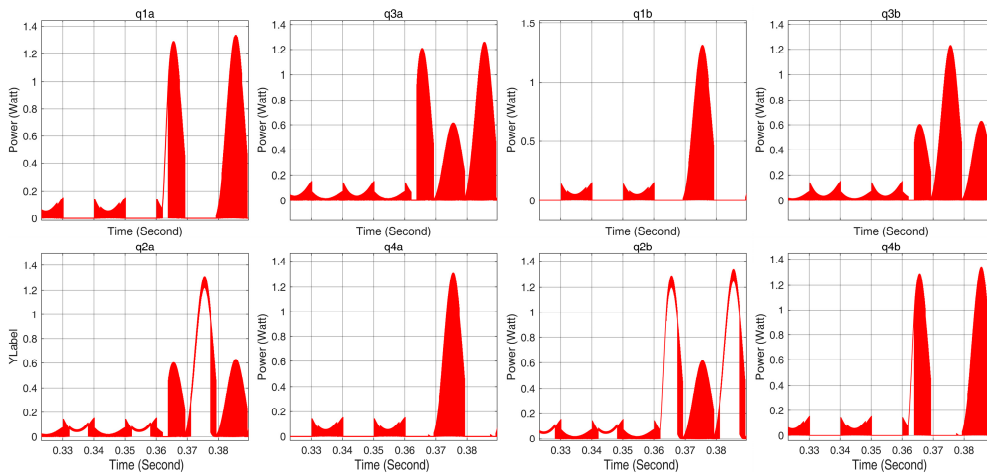


Figure 6. Switching losses for all switches in the proposed system.

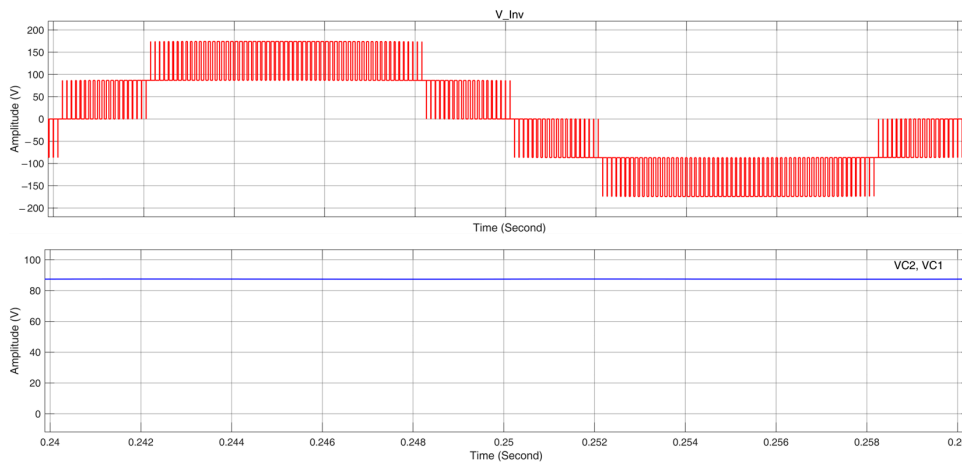


Figure 7. Inverter and main capacitors voltage waveforms.

4.1. System Simulation When PV Array Is Idle

When the system is simulated for nonlinear load while the PV array is idle, the load power components are compensated, and the grid supplies only the load’s real power (see Figure 8).

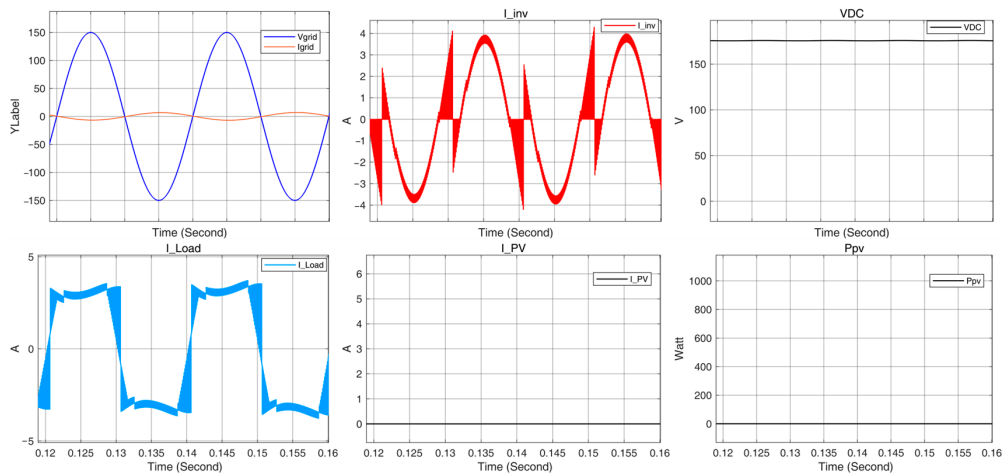
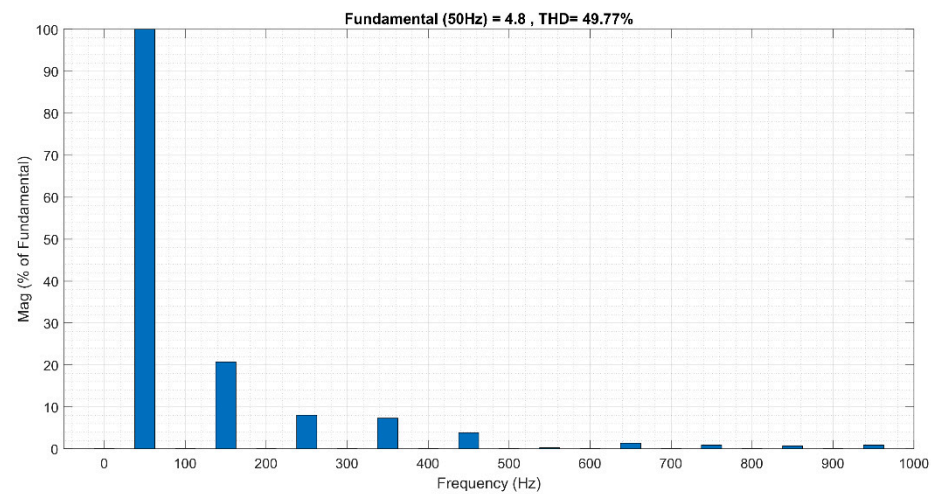
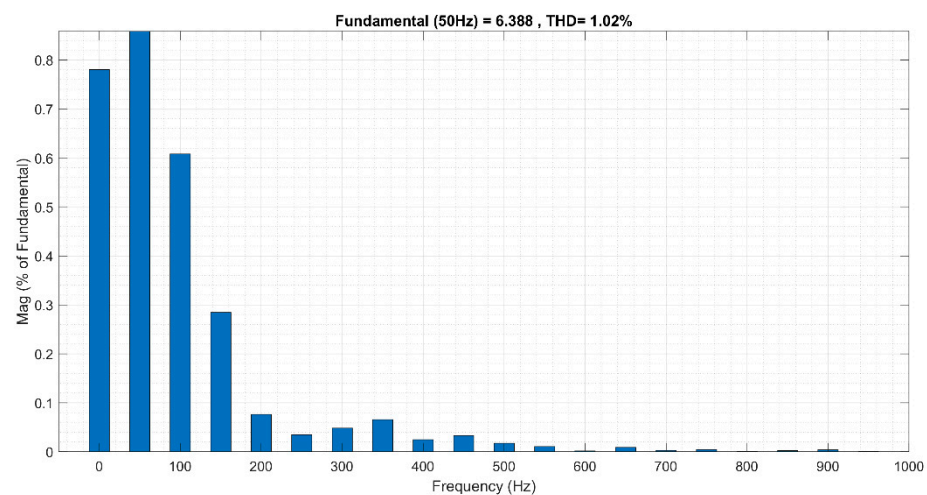


Figure 8. System simulation results when the PV array is idle.

The load and grid current FFT analysis are shown in Figures 9 and 10, respectively. As shown in Figure 9, the load current total harmonics distortion THD is 49.77%.



**Figure 9.** Load current FFT analysis.



**Figure 10.** Grid current FFT when PV array is idle.

While the grid current THD is 1.02%, as shown in Figure 10.

#### 4.2. System Simulation When PV Power = Load Power

In this case, the total real power produced by the PV array is equal to the load real power. This case is the more complex case because the grid current is near zero, and this makes the compensation process more difficult. System simulation results for this case are shown in Figure 11.

The grid current THD for this case is 3.67%, as shown in Figure 12.

#### 4.3. System Simulation When PV Power Is More Than the Load Real Power

In this case, the real power produced by the PV array is greater than the load of real power. Therefore, the grid current direction is from the converter to the grid (the grid is treated as an energy storage system). The simulation results are shown in Figure 13.

While the grid current FFT analysis is shown in Figure 14, the THD in the grid current in this case is 0.62%.

For all simulated cases, the grid current THD is less than 5% while the system keeps working in minimum switching losses in spite of using the PWM technique, which is

known as a high-switching-losses technique. Figure 15 shows the switching losses for each IGBT in the F-type inverter for all simulated cases.

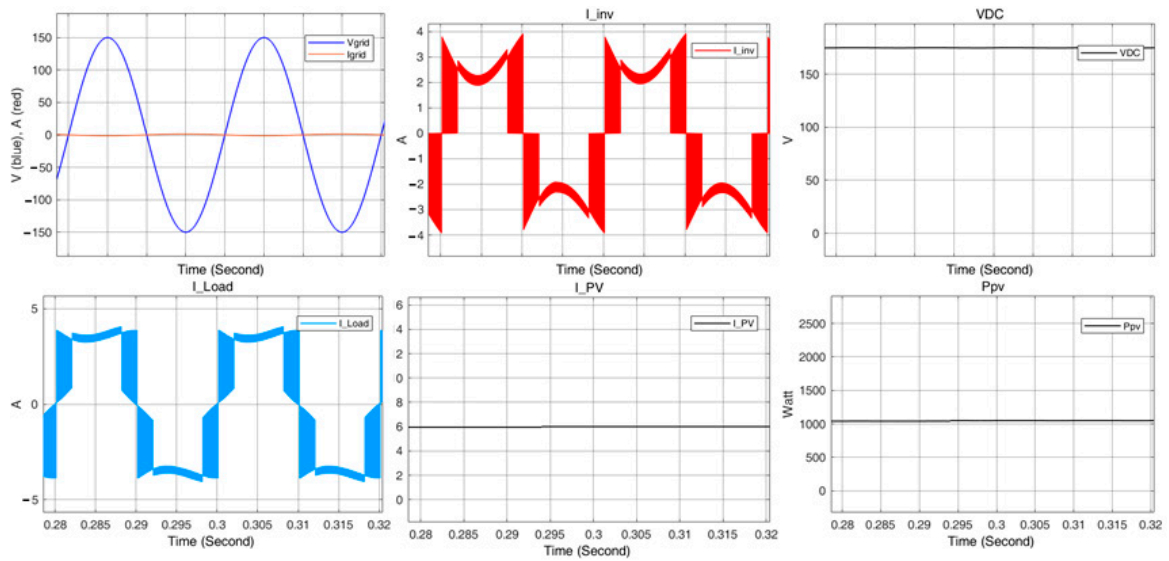


Figure 11. System simulation results when  $P_{pv} = P_{load}$ .

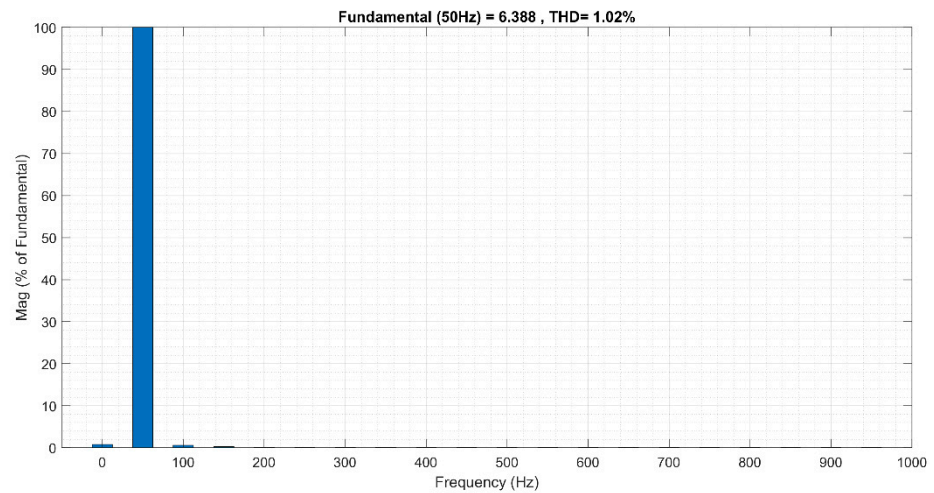


Figure 12. Grid current FFT when  $P_{pv} = P_{load}$ .

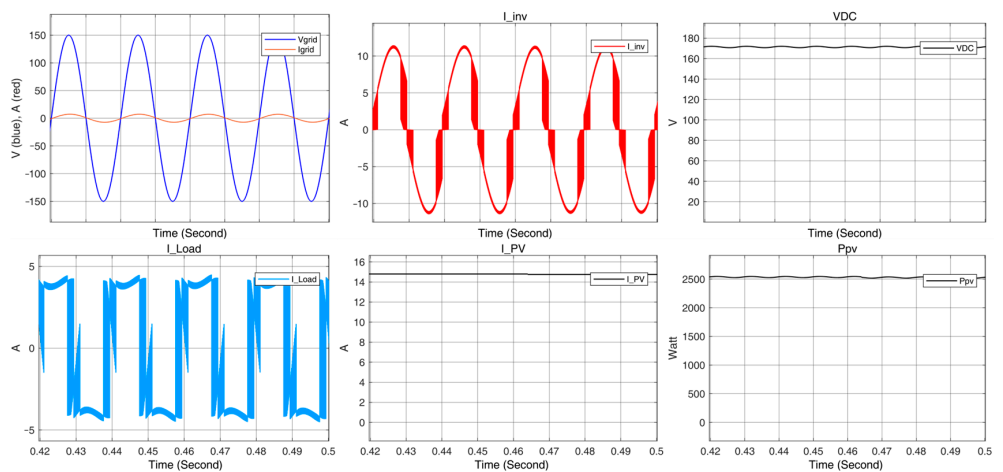


Figure 13. System simulation results when  $P_{pv} > P_{load}$ .

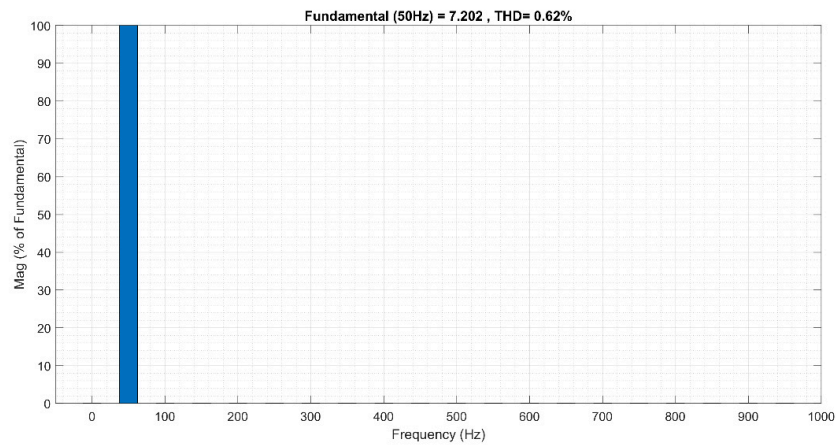


Figure 14. Grid current FFT when  $P_{pv} > P_{load}$ .

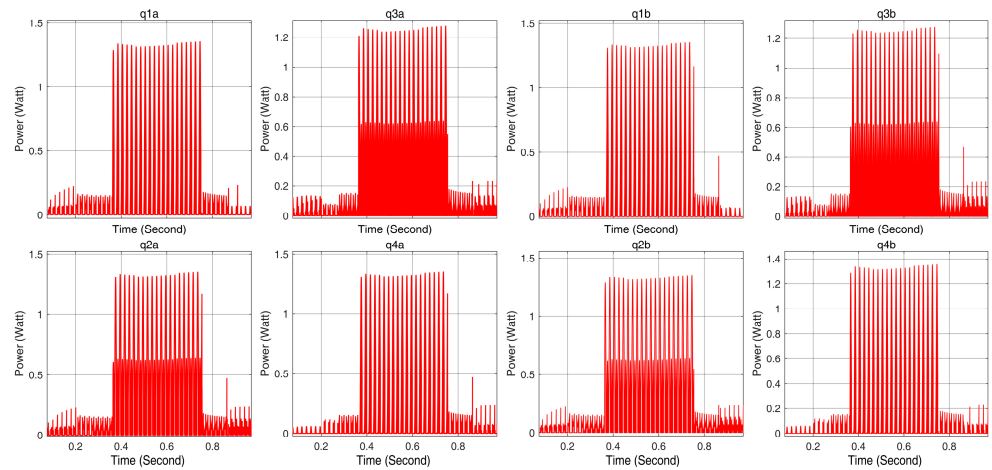


Figure 15. Switching losses for the proposed system in all simulated cases.

As shown in Figure 15, it is clear that 50% of the IGBTs are working in zero voltage switching ZVS without using any additional components or switching frequency reduction.

Additionally, the main advantage of the F-type inverter is kept which is only 25% of the IGBTs under high DC voltage equal to the PV array DC voltage, while the other 75% are working with  $V_{dc}/2$ . Figure 16 shows the voltage stress and current through each IGBT.

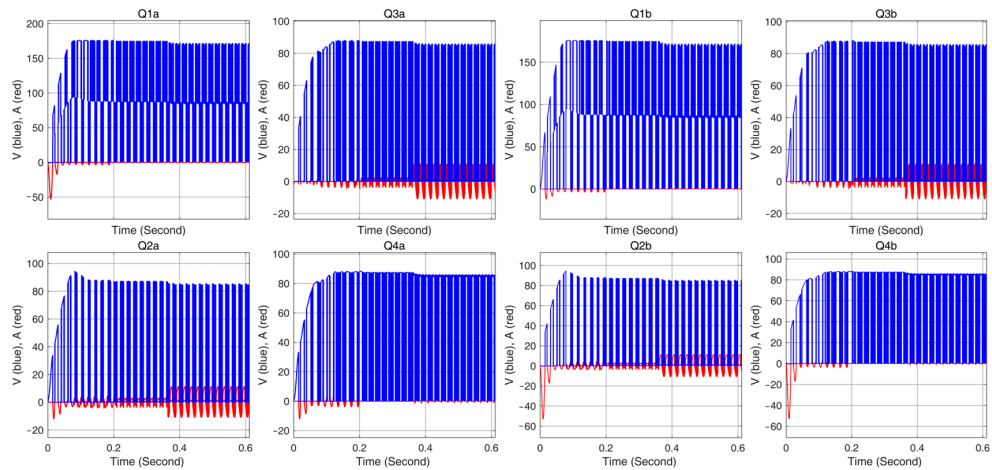


Figure 16. Voltage and current are applied to each IGBT in the F-type inverter.

#### 4.4. System Simulation for Sudden Load Change Case

The effect on system response when the load changes suddenly is shown in Figure 17. It is clear the system response for load change requires less than one cycle ( $<0.02$  s). Load change occurs in “0.3 s” and continues for 0.1 s, then ends in “0.4 s”. The grid current curve, as shown in Figure 17, shows the change durations that are zoomed in to focus on the response. Before 0.3 seconds, the load capacity is less than the power produced by the PV array, while in the duration (0.3–0.4) second, the load capacity exceeds the power produced by the PV array; therefore, the grid current magnitude and direction are changed depending on the load change. The system performance stays stable, and the grid current is still as defined in Equations (6) and (7).

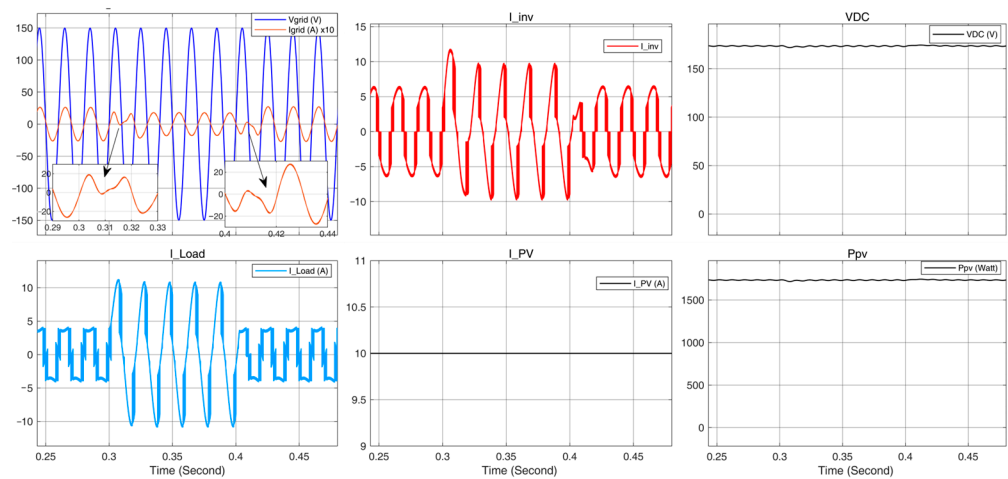


Figure 17. System response in load sudden change.

#### 4.5. PV Array Power Change Effect

The variation of the generated power by the PV array does not affect the system performance because the system response is faster than the PV power change. Figure 18 shows the response of the system under PV array power change.

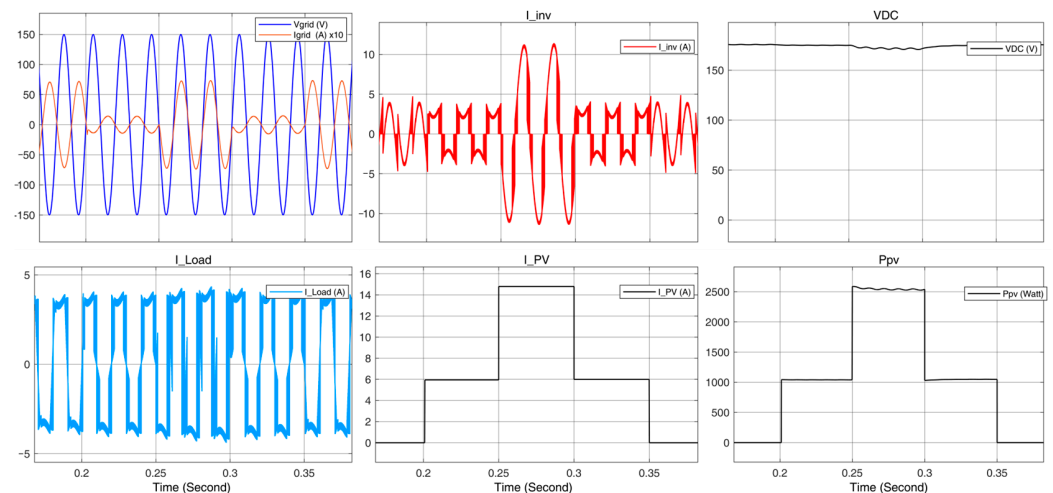


Figure 18. PV array power change effect on system performance.

As shown in Figure 18, the grid current amplitude and direction depend on the difference between the load real power and the PV array real power. The grid current curve in Figure 18 is scaled ( $\times 10$ ) to make it accurately readable.

#### 4.6. Comparative Study

The proposed control method used in controlling both F-type and T-type inverters in the same operating conditions; the simulation results comparisons are listed in Table 2. The simulation results show that the PV array utilization of the F-type inverter under the proposed control scheme is better than that of the T-type inverter under the same control scheme. When the PV array is idle, there is no real power produced from the PV array; therefore, the grid current must be equal to the load current real part. In the F-type inverter case, the grid current is less than that in the case of the T-type inverter. When the PV array current reaches the load current real part (6 A) the grid current in the case of F-type is less than that of T-type. Finally, when the PV array current became greater than the load current real part, in this case, the current flows from the inverter side to the grid side, and also, the F-type utilized the PV array current best than the T-type inverter.

**Table 2.** Performance comparison for F-type and T-type inverters under the proposed control scheme.

I PV (A)	0	6	14.75
I grid (F-type) (A)	6.98	1.32	7.145
I grid (T-type) (A)	7.43	1.64	6.87
THD (F-type) (%)	0.73	3.58	0.62
THD (T-type) (%)	0.57	2.45	0.54

The THD for grid current produced by both inverters is in the accepted limit, while the T-type inverter current THD is the little best.

#### 5. Conclusions

In this article, an innovative control method is proposed to control a grid-connected F-type inverter powered by a solar cell system with a non-linear load. The simulation results show the high performance of the proposed system in constant and dynamic operation modes. The total harmonic distortion THD in injected or absorbed grid current is less than 4%, even in the worst operating case when the PV array real power equals the load real power. Additionally, the proposed control system was simulated with a T-type inverter; the simulation results are compared to verify the performance of the proposed system. The proposed grid-connected F-type PV-powered inverter GCFTPVI operates with two switching modes depending on the main capacitors' voltages to keep the voltage balance. In addition, the switching losses are very low because the proposed control method satisfies zero voltage switching ZVS in 50% of the inverter switches without any components addition, and that leads to reduced cost keeping.

The proposed GCFTPVI can be considered a suitable technique for home PV applications thanks to its ability to compensate the load power components and inject the real power from the PV array instantaneously with minimum THD and switching losses.

**Author Contributions:** Conceptualization, R.A.; methodology, A.K. and R.A.; software, A.K.; validation, R.A. and M.B.S.; formal analysis, A.T.; investigation, A.S.; resources, R.A. and A.K.; data curation, A.K.; writing—original draft preparation, R.A.; writing—review and editing, R.A., M.B.S. and A.T.; supervision, A.S. All authors have read and agreed to the published version of the manuscript.

**Funding:** This research received no external funding.

**Data Availability Statement:** The analyzed data is the simulation results, and it is included in the article.

**Conflicts of Interest:** The authors declare no conflict of interest.

## References

1. Çelik, D. Lyapunov based harmonic compensation and charging with three phase shunt active power filter in electrical vehicle applications. *Int. J. Electr. Power Energy Syst.* **2022**, *136*, 107564. [[CrossRef](#)]
2. Barreto-Parra, G.F.; Cortés-Caicedo, B.; Montoya, O.D. Optimal Integration of D-STATCOMs in Radial and Meshed Distribution Networks Using a MATLAB-GAMS Interface. *Algorithms* **2023**, *16*, 138. [[CrossRef](#)]
3. Abdullah, R.D.; Khalaf, A.A.; Drobic, G. Power Components Compensation by Utilizing Pv Converter Functions. *Des. Eng.* **2021**, *7*, 4913–4925.
4. Kalla, U.K.; Kaushik, H.; Singh, B.; Kumar, S. Adaptive Control of Voltage Source Converter Based Scheme for Power Quality Improved Grid-Interactive Solar PV–Battery System. *IEEE Trans. Ind. Appl.* **2019**, *56*, 787–799. [[CrossRef](#)]
5. Ji, Y.; Yuan, Z.; Zhao, J.; Wang, Y.; Zhao, Y. Overall control scheme for VSC-based medium-voltage DC power distribution networks. *IET Gener. Transm. Distrib.* **2018**, *12*, 1438–1445. [[CrossRef](#)]
6. Omer, P.; Kumar, J.; Surjan, B.S. A Review on Reduced Switch Count Multilevel Inverter Topologies. *IEEE Access* **2020**, *8*, 22281–22302. [[CrossRef](#)]
7. Bana, P.R.; Panda, K.P.; Naayagi, R.T.; Siano, P.; Panda, G. Recently developed reduced switch multilevel inverter for renewable energy integration and drives application: Topologies, comprehensive analysis and comparative evaluation. *IEEE Access* **2019**, *7*, 54888–54909. [[CrossRef](#)]
8. Vijeh, M.; Rezanejad, M.; Samadaei, E.; Bertilsson, K. A General Review of Multilevel Inverters Based on Main Submodules: Structural Point of View. *IEEE Trans. Power Electron.* **2019**, *34*, 9479–9502. [[CrossRef](#)]
9. Odeh, C.I.; Lewicki, A.; Morawiec, M.; Kondratenko, D. Three-Level F-Type Inverter. *IEEE Trans. Power Electron.* **2021**, *36*, 11265–11275. [[CrossRef](#)]
10. Sefa, I.; Ozdemir, S.; Komurcugil, H.; Altin, N. Comparative study on Lyapunov-function-based control schemes for single-phase grid-connected voltage-source inverter with LCL filter. *IET Renew. Power Gener.* **2017**, *11*, 1473–1482. [[CrossRef](#)]
11. Shadoul, M.; Yousef, H.; Abri, R.; Al-Hinai, A. Adaptive Fuzzy Approximation Control of PV Grid-Connected Inverters. *Energies* **2021**, *14*, 942. [[CrossRef](#)]
12. Qi, Y.; Deng, H.; Liu, X.; Tang, Y. Synthetic Inertia Control of Grid-connected Inverter Considering the Synchronization Dynamics. *IEEE Trans. Power Electron.* **2021**, *37*, 1411–1421. [[CrossRef](#)]
13. Azab, M. A finite control set model predictive control scheme for single-phase grid-connected inverters. *Renew. Sustain. Energy Rev.* **2021**, *135*, 110131. [[CrossRef](#)]
14. Shieh, J.-J.; Hwu, K.-I.; Li, Y.-Y. A Single-Voltage-Source Class-D Boost Multi-Level Inverter with Self-Balanced Capacitors. *Energies* **2022**, *15*, 4082. [[CrossRef](#)]
15. Srinivasan, G.K.; Rivera, M.; Loganathan, V.; Ravikumar, D.; Mohan, B. Trends and Challenges in Multi-Level Inverter with Reduced Switches. *Electronics* **2021**, *10*, 368. [[CrossRef](#)]
16. Deffaf, B.; Debouche, N.; Benbouhenni, H.; Hamoudi, F.; Bizon, N. A New Control for Improving the Power Quality Generated by a Three-Level T-Type Inverter. *Electronics* **2023**, *12*, 2117. [[CrossRef](#)]
17. Gu, X.; Xu, W.; Zhang, G.; Chen, W.; Jin, X. Three-Level Inverter-PMSM Model Predictive Current Control Based on the Extended Control Set. *Electronics* **2023**, *12*, 557. [[CrossRef](#)]
18. Kumar, A.; Verma, V. Performance enhancement of single-phase grid-connected PV system under partial shading using cascaded multilevel converter. *IEEE Trans. Ind. Appl.* **2018**, *54*, 2665–2676. [[CrossRef](#)]
19. Cecati, C.; Ciancetta, F.; Siano, P. A Multilevel Inverter for Photovoltaic Systems with Fuzzy Logic Control. *IEEE Trans. Ind. Electron.* **2010**, *57*, 4115–4125. [[CrossRef](#)]
20. Shuvo, S.; Hossain, E.; Islam, T.; Akib, A.; Padmanaban, S.; Khan, M.Z.R. Design and hardware implementation considerations of modified multilevel cascaded H-bridge inverter for photovoltaic system. *IEEE Access* **2019**, *7*, 16504–16524. [[CrossRef](#)]
21. Naghavi, F.; Toliyat, H. Grid-connected Soft Switching Partial Resonance Inverter for Distributed Generation. In Proceedings of the 2022 IEEE 31st International Symposium on Industrial Electronics (ISIE), Anchorage, Alaska, 1–3 June 2022; pp. 927–932.
22. Bayhan, S.; Komurcugil, H. Sliding-mode control strategy for three-phase three-level T-type rectifiers with DC capacitor voltage balancing. *IEEE Access* **2020**, *8*, 64555–64564. [[CrossRef](#)]
23. Alepuz, S.; Busquets-Monge, S.; Nicolás-Apruzzese, J.; Filbà-Martínez, À.; Bordonau, J.; Yuan, X.; Kouro, S. A Survey on Capacitor Voltage Control in Neutral-Point-Clamped Multilevel Converters. *Electronics* **2022**, *11*, 527. [[CrossRef](#)]
24. Marchesoni, M.; Tenca, P. Diode-clamped multilevel converters: A practicable way to balance DC-link voltages. *IEEE Trans. Ind. Electron.* **2002**, *49*, 752–765. [[CrossRef](#)]
25. Michalec, M.; Jasiński, M.; Sikorski, T.; Leonowicz, Z.; Jasiński, Ł.; Suresh, V. Impact of Harmonic Currents of Nonlinear Loads on Power Quality of a Low Voltage Network—Review and Case Study. *Energies* **2021**, *14*, 3665. [[CrossRef](#)]
26. Stanelyte, D.; Radziukynas, V. Review of Voltage and Reactive Power Control Algorithms in Electrical Distribution Networks. *Energies* **2020**, *13*, 58. [[CrossRef](#)]
27. Sharma, R.; Singh, A.; Jha, A.N. Performance evaluation of tuned PI controller for power quality enhancement for linear and non linear loads. In Proceedings of the International Conference on Recent Advances and Innovations in Engineering (ICRAIE-2014), Jaipur, India, 9–11 May 2014; pp. 1–6.
28. Woyte, A.; Van Thong, V.; Belmans, R.; Nijs, J. Voltage fluctuations on distribution level introduced by photovoltaic systems. *IEEE Trans. Energy Convers.* **2006**, *21*, 202–209. [[CrossRef](#)]

29. Faiz, J.; Shahgholian, G. Modeling and simulation of a three-phase inverter with rectifier-type nonlinear loads. *Armen. J. Phys.* **2009**, *2*, 307–316.
30. Kadnekar, V. Permanent Magnet Synchronous Motor Drive System Utilizing DQ Transformation. Ph.D. Thesis, California State University, Northridge, CA, USA, 2018.
31. Monfared, M.; Sanatkar, M.; Golestan, S. Direct active and reactive power control of single-phase grid-tie converters. *IET Power Electron.* **2012**, *5*, 1544–1550. [[CrossRef](#)]
32. Chattopadhyay, S.; Mitra, M.; Sengupta, S. Clarke and park transform. In *Electric Power Quality*; Springer: Dordrecht, The Netherlands, 2011; pp. 89–96.

**Disclaimer/Publisher's Note:** The statements, opinions and data contained in all publications are solely those of the individual author(s) and contributor(s) and not of MDPI and/or the editor(s). MDPI and/or the editor(s) disclaim responsibility for any injury to people or property resulting from any ideas, methods, instructions or products referred to in the content.